Temperature Enhancement of Thermal Hall Conductance Quantization

I. C. Fulga,[1] Yuval Oreg,[2] Alexander D. Mirlin,[3,4,5] Ady Stern,[2] and David F. Mross[2]
[1]*IFW Dresden and Würzburg-Dresden Cluster of Excellence, Helmholtzstrasse 20, 01069 Dresden, Germany*
[2]*Department of Condensed Matter Physics, Weizmann Institute of Science, Rehovot 76100, Israel*
[3]*Institute for Quantum Materials and Technologies, Karlsruhe Institute of Technology, 76021 Karlsruhe, Germany*
[4]*Institut für Theorie der Kondensierten Materie, Karlsruhe Institute of Technology, 76128 Karlsruhe, Germany*
[5]*L. D. Landau Institute for Theoretical Physics RAS, 119334 Moscow, Russia*

(Received 3 July 2020; accepted 9 November 2020; published 2 December 2020)

The quest for non-Abelian quasiparticles has inspired decades of experimental and theoretical efforts, where the scarcity of direct probes poses a key challenge. Among their clearest signatures is a thermal Hall conductance with quantized half-integer value in units of $\kappa_0 = \pi^2 k_B^2 T/3h$ (T is temperature, h the Planck constant, k_B the Boltzmann constant). Such values were recently observed in a quantum-Hall system and a magnetic insulator. We show that nontopological "thermal metal" phases that form due to quenched disorder may disguise as non-Abelian phases by well approximating the trademark quantized thermal Hall response. Remarkably, the quantization here *improves* with temperature, in contrast to fully gapped systems. We provide numerical evidence for this effect and discuss its possible implications for the aforementioned experiments.

DOI: 10.1103/PhysRevLett.125.236802

Introduction.—Measurements of the electronic or thermal Hall effect are powerful experimental techniques for identifying topologically ordered phases and their fractional quasiparticles [1]. An electronic Hall conductance sharply quantized to a noninteger value (in units of e^2/h, with e the electron charge) is intimately related to the existence of fractionally charged quasiparticles [2]. Similarly, a quantized noninteger thermal Hall conductance κ_{xy} reflects excitations with non-Abelian braiding properties [3–8]. While the electronic Hall effect has been routinely measured for several decades [9], precise measurements of the thermal Hall effect in solid-state systems have been achieved only recently [10–14]. Remarkably, experiments on two completely different systems found half-integer values, indicative of so-called Ising anyons. The first is a two-dimensional electron gas in a perpendicular magnetic field at filling factor $\nu = 5/2$ with a thermal Hall conductance $\kappa_{xy} = 5/2$ [12]. The second is the magnetic insulator α-$RuCl_3$, where $\kappa_{xy} = 1/2$ per layer was measured in an applied magnetic field [13].

The level of quantization observed in the thermal Hall measurements is significantly below the one in their electronic analogs. This may be due to heat leakage from the measured system to its environment, e.g., via phonons. Our work focuses on an additional, intrinsic property that may be particularly relevant to situations with half-integer κ_{xy} under experimental conditions, which necessarily include sample imperfections, i.e., disorder [15–17]. In the context of both the quantum Hall effect and α-$RuCl_3$, the half-integer κ_{xy} results from topological $p_x \pm ip_y$ pairing [3,18] (and consequently chiral edge Majoranas) of *emergent* fermions: composite fermions and spinons, respectively. In both cases, the fermions are minimally coupled to an emergent gauge field, which acquires a Higgs mass and thereby eliminates the phase mode of the emergent-fermion superconductor. The effective low-energy theory thus falls into class D in the Altland-Zirnbauer classification (AZ) [19], which permits a delocalized *thermal metal* phase [5,20–28]; see Supplemental Material for more background [29]. This property is sharply distinct from, e.g., the symmetry class A of electrons in the quantum Hall effect, which always localizes unless the system is at a topological phase transition [31]. The thermal metal also crucially differs from the metallic state formed from electrons that weakly antilocalize due to spin-orbit coupling [32–35]: It exhibits delocalized states only at energy $E = 0$ where particle-hole symmetry holds; at any nonzero energy it crosses over into class A at long length scales and all states localize.

In this work we demonstrate remarkable consequences of these localization characteristics: As temperature increases, the longitudinal thermal conductance *decreases* and vanishes for thermodynamically large systems. Concomitantly, the thermal Hall conductance becomes better quantized. This somewhat counterintuitive behavior arises because thermal conductance is determined not solely by the delocalized $E = 0$ states, but by all states in an energy window $\sim T$. Since almost all of these states are localized, the thermal conductance vanishes. This localization behavior is similar to the one exhibited by electrons near an integer quantum Hall plateau transition. There, an infinitely sharp transition at $T \neq 0$ is predicted on the

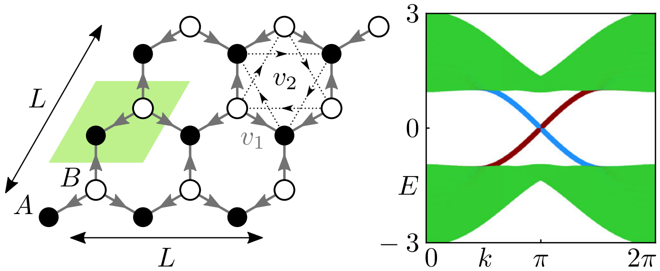

FIG. 1. Left: The unit cell of the model (shaded area) contains two sites, indicated by solid and open circles, each hosting a single Majorana mode. The signs of (i times) the nearest-neighbor hopping v_1 and next-nearest-neighbor hoppings v_2 are indicated by the direction of arrows on the corresponding bonds. Right: Band structure of the model in a ribbon geometry, infinite in the horizontal direction and consisting of 30 unit cells in the vertical direction, using $v_1 = 1$ and $v_2 = -0.2$. Bulk states are shown in green; states on the top and bottom edges are shown in red and blue, respectively.

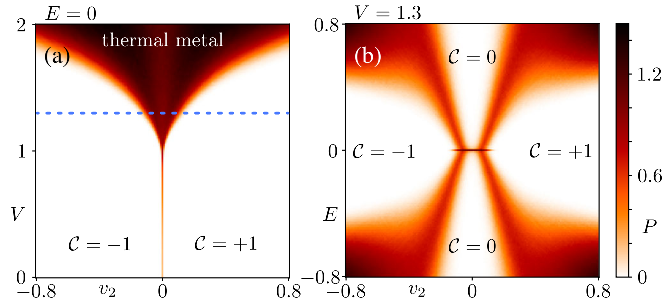

FIG. 2. The average transmission of a 80×80 unit cells system, computed using 1000 disorder realizations. (a) The horizontal axis is v_2 and the vertical axis is disorder strength V. The topological transition between phases with Chern numbers $\mathcal{C} = \pm 1$ evolves into a thermal metal phase with increasing disorder strength. The dashed blue line indicates $V = 1.3$. (b) For fixed $V = 1.3$, the average transmission is plotted as a function of v_2 and energy E. Away from the particle-hole symmetric line, $E = 0$, the thermal metal phase disappears; it is replaced by topologically trivial insulators ($\mathcal{C} = 0$).

single-particle level, but interactions render the width of the transition finite [36]. In the present case, interactions allow thermal metal behavior to persist over a finite temperature window. We will comment on the role of interactions towards the end of our discussion.

Model and symmetries.—For concreteness, we frame our discussion in the language of the quantum Hall plateau at $\nu = 5/2$. At energies below the charge gap, we model the system by a quadratic Bogoliubov–de Gennes Hamiltonian. We require that it exhibits two topological phases that are related by time-reversal symmetry (TRS) and permits a thermal metal phase. (TRS of composite fermions corresponds to particle-hole symmetry of electrons within a single Landau level [37], which relates the Pfaffian and anti-Pfaffian phases [38,39].)

A minimal model that satisfies these criteria is given by a honeycomb lattice with a single Majorana fermion per site as shown in Fig. 1 [18]. (Such a model also arises microscopically in the Kitaev spin model below the vison gap. For a discussion of the thermal conductance at higher energies, see Ref. [40].) The Hamiltonian reads

$$H = iv_1 \sum_{\langle j,k \rangle} \gamma_j \gamma_k + iv_2 \sum_{\langle\langle j,k \rangle\rangle} \gamma_j \gamma_k, \qquad (1)$$

where γ_j is a Majorana operator on site j, $\langle j, k \rangle$ denotes directed bonds from B to neighboring A sites, and $\langle\langle j, k \rangle\rangle$ clockwise next-nearest neighbor bonds (see Fig. 1). We set $v_1 = 1$ throughout the following, expressing all energy scales relative to it.

The Hamiltonian Eq. (1) obeys particle-hole (PH) symmetry. Writing $H = \boldsymbol{\gamma}^T \mathcal{H} \boldsymbol{\gamma}$, with $\boldsymbol{\gamma}$ a column vector of Majorana operators, the PH symmetry can be expressed as $\mathcal{H} = -\mathcal{H}^*$, such that the system belongs to class D. For $v_2 = 0$, the model features an additional TRS consisting of complex conjugation followed by a sign change of the wave function on one of the two sublattices, and thus falls into the symmetry class labeled BDI in the AZ classification. Here, the spectrum is gapless, with two linearly dispersing Majorana cones at momenta K and K'. A nonzero mass term v_2 results in a gapped phase with Chern number $\mathcal{C} = \mathrm{sgn}(v_2)$.

Notice that TRS, which is present for $v_2 = 0$, implies a vanishing thermal Hall conductance, while the corresponding particle-hole symmetry in the first excited Landau level requires the value $5/2$ [41]. Consequently, a "background" contribution of $5/2$ must be added to interpret results for the model system in the quantum Hall context, i.e., $\kappa_{xy}^{\mathrm{QH}} = \kappa_{xy} + 5/2$. The TRS breaking parameter v_2 describes either Landau level mixing or the deviations of ν from $5/2$.

Zero-temperature phase diagram.—We now introduce random hopping disorder and examine the localization properties near the topological phase transition of the clean system as a function of disorder strength V and energy E. Specifically, we replace $v_i \to v_i + \delta v_i$ with δv_1 from a uniform distribution $[-V, V]$ and δv_2 independently from $[-V/10, V/10]$. We numerically compute the energy-dependent transmission probability $P(E)$ for a cylindrical $L \times L$ system with zigzag edges. See Supplemental Material for details [29].

In Fig. 2(a) we show the transmission at zero energy as a function of v_2 and disorder strength. At weak disorder, the insulating $\mathcal{C} = \pm 1$ phases remain separated by a direct plateau transition; see also discussion in Refs. [20,24–27]. When $V \gtrsim 1$, however, a delocalized phase develops around $v_2 = 0$. This is a disorder-induced thermal metal where $P(E = 0)$ increases logarithmically with system size; see Supplemental Material [29]. Further increasing the disorder strength enlarges the thermal metal region. In Fig. 2(b), we plot the energy-dependent transmission probability at fixed disorder strength $V = 1.3$, where the thermal metal is well developed. We observe that the metal is only present at $E = 0$. This is the expected result based on weak antilocalization in the PH symmetric case, $E = 0$, and weak localization for any $E \neq 0$. The latter case features direct insulator-to-insulator transitions, with a trivial, $C = 0$ phase between the topological $\mathcal{C} = \pm 1$ phases.

We have further observed that the crossover regions in Fig. 2(b) (the regions with nonzero transmission) shrink with increasing system size and grow with δv_2 disorder. The former is required due to the absence of metallic phases in class A, i.e., for $E \neq 0$. To understand the latter, recall that for $v_2 = \delta v_2 = 0$ the model is in class BDI, which only permits a critical-metal phase (without antilocalization, see Supplemental Material [29]), distinct from the class-D thermal metal [26]. Gradually introducing δv_2 disorder allows the formation of a growing thermal metal phase at $E = 0$ and, in finite systems, a corresponding crossover at $E \neq 0$. For the numerically accessible system sizes, we find that the $C = 0$ insulator fully disappears into a smooth crossover for approximately equal v_1 and v_2 disorder.

At $E \neq 0$ the system is in class A and thus always localizes. For small energies, the localization length is determined by the crossover between weak antilocalization of class D and weak localization of class A [25]. At distances below the diffusion length $L_E = \sqrt{D/E}$, with D the diffusion constant, the interference of electron and hole trajectories gives rise to a logarithmic increase of the conductance. At scales above L_E, this interference is suppressed; the system behaves as a class-A conductor, which tends to localize. The localization length $\xi(E)$ can be computed as for the case of spin-orbit coupled electrons in a weak magnetic field, which features a similar crossover between weakly antilocalizing class AII and weakly localizing class A [42]. We find

$$\xi(E) = \frac{\ell_0}{\sqrt{E}} \exp\left(\frac{1}{4} \ln^2 \frac{1}{E}\right), \qquad (2)$$

with ℓ_0 the mean free path (see Supplemental Material [29]). Both $L_E, \xi(E)$ depend on energy and diverge with decreasing energy, with asymptotically $\xi(E) \gg L_E$. In a finite-size system it is further useful to define two crossover energy scales: $E_L \propto L^{-2}$, for which $L_E = L$, and E_c, for which $\xi = L$. States with energies below E_L are weakly antilocalizing, states with energies between E_L and E_c are characterized by weak localization, whereas strong localization sets in above E_c.

Finite temperature effects.—The above discussion and the results presented in Fig. 2 suggest that the dimensionless thermal conductance tensor κ changes qualitatively as temperature is swept past either crossover scale. (In infinite systems $E_c = E_L = 0$.) To test this expectation, we compute κ_{xx} and κ_{xy} in a six-terminal transport geometry, where

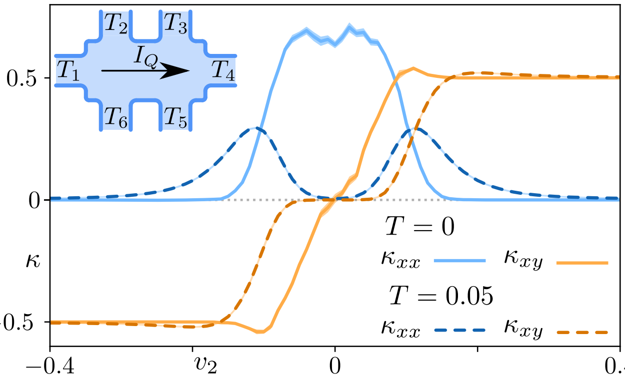

FIG. 3. The dimensionless longitudinal and transverse thermal conductances (blue, orange) are computed in a six-terminal geometry (inset) at $T = 0$ and $T = 0.05$ (solid, dashed). We use a rectangular system composed of 80 zigzag chains in the vertical direction and 160 hexagonal plaquettes in the horizontal direction, and average over 1000 disorder realizations ($V = 1.3$), with line thickness indicating the error bars. The thermal metal phase present in the $v_2 = 0$ region of the plot is converted into an insulating phase at nonzero temperature, leading to a quantized plateau in both longitudinal and transverse conductance. Notice the smaller error bars in the finite-temperature curves, which occur because the energy integral Eq. (4) provides additional disorder averaging.

both can be obtained in the same numerical simulation. Terminals are numbered from 1 to 6, as shown in the inset of Fig. 3. The scattering matrix has a 6×6 block structure, with blocks $\mathfrak{s}_{ij}$ containing the probability amplitudes for transmission from lead i to lead j.

All reservoirs are kept at equal chemical potentials, and terminals 1 and 4 are temperature-biased as $T_{1,4} = \pm \Delta T/2$ relative to the base temperature T. Consequently, a heat current $I_Q = I_1 = -I_4$ flows through the system. The remaining terminals are connected to thermometers, such that $I_{2,3,5,6} = 0$. Setting $h = k_B = 1$, temperatures and heat current are related via [43]

$$\begin{pmatrix} I_Q \\ 0 \\ 0 \\ -I_Q \\ 0 \\ 0 \end{pmatrix} = M \begin{pmatrix} \Delta T/2 \\ T_2 \\ T_3 \\ -\Delta T/2 \\ T_5 \\ T_6 \end{pmatrix}, \qquad (3)$$

where the matrix M is given by

$$M_{ij} = \int_0^\infty \frac{E^2}{T} \left(-\frac{\partial f(E,T)}{\partial E} \right) [\delta_{ij} N_j - \mathrm{tr}(\mathfrak{s}_{ij}^\dagger \mathfrak{s}_{ij})] dE, \qquad (4)$$

with δ_{ij} denoting the Kronecker delta, N_j the number of modes in lead j, and $f(E,T) = 1/(1 + e^{E/T})$ the Fermi-Dirac distribution. Notice that the scattering matrix depends on energy, which results in a nontrivial temperature dependence of M. We numerically compute the matrix M for each disorder realization, and insert it into Eq. (3) to calculate the elements of the thermal resistance tensor, R_{xx} and R_{xy}. We define $R_{xx} = (T_2 - T_3)/I_Q$, whereas for R_{xy} we average over the temperature drop between terminals 2 and 6 and between terminals 3 and 5: $R_{xy} = (T_2 - T_6 + T_3 - T_5)/(2I_Q)$ to reduce geometric effects. The dimensionless conductance tensor κ is then obtained by inverting R and dividing by κ_0. In Fig. 3 we plot the disorder-averaged components κ_{xx} and κ_{xy} at $T = 0$ (solid lines) and $T = 0.05$ (dashed lines). We observe that at zero temperature the transition between $\mathcal{C} = \pm 1$ phases in which $\kappa_{xy} = \pm 0.5$ occurs via an intermediate thermal metal phase. This is signaled by a large peak in κ_{xx} and a nonquantized κ_{xy}. At finite temperature the thermal metal peak is replaced by an intermediate plateau of $\kappa_{xx/xy} \approx 0$ in the small $|v_2|$ region of the plot. At large $|v_2|$, however, the dimensionless thermal conductance remains qualitatively unchanged, with $\kappa_{xy} \to \pm 0.5$ and $\kappa_{xx} \to 0$, since the insulating phases with $\mathcal{C} = \pm 1$ extend to an energy range larger than temperature (see Fig. 2).

To understand the observed behavior, notice that temperature-dependent factor in the integrand of Eq. (4) is sharply peaked at energies around T and becomes a delta function at zero temperature. For temperatures below the crossover energy scale E_c, the main contribution to the integral comes from extended states and κ_{xx} is large while κ_{xy} is approximately linear in v_2. The low-temperature regime subdivides into $T < E_L$, where κ_{xx} is determined by the metallic transmission probability $P(E \approx 0)$ and $E_L < T < E_c$, where weak localization modifies this result; see Supplemental Material [29]. At temperatures above E_c, strong localization becomes operative and leads to $\kappa_{xx} \to 0$, as we observe numerically. This insulating behavior is accompanied by an emergent intermediate plateau in κ_{xy}, as shown in Figs. 3 and 4(a).

Effect of interactions.—Both the numerical simulations and the σ-model treatment were performed within quadratic fermionic Hamiltonians, where transport is fully phase coherent. We now qualitatively discuss how interactions change these results, focusing on the fractional quantum Hall effect at $\nu = 5/2$. We consider a thermodynamically large system, $L \to \infty$, and focus on phase-breaking of the emergent fermions. The presence of phonons leads to another channel for heat transport, which is expected to follow a power law of $\kappa^{\mathrm{ph}} \propto T^5$ [44]. Its contribution is suppressed at low temperatures, as indeed observed in the experiment [12,13].

The phase-breaking interactions of an interfering particle with its environment introduce a dephasing length L_ϕ [45], which diverges with decreasing temperature, presumably following a power law. This length should be compared to the diffusion length L_E and the localization length $\xi(E)$ [defined near Eq. (2)]. The relevant energy is the temperature, since the chemical potential is zero.

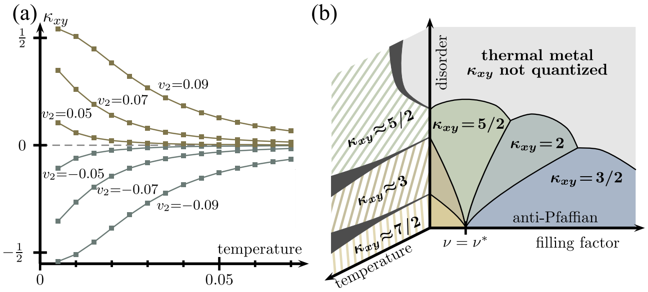

FIG. 4. (a) The numerically computed thermal conductance shows order-unity variations with v_2 at low temperatures. At higher temperatures it approaches the time-reversal symmetric value $\kappa_{xy} = 0$ with very weak dependence on $v_2 \in [-0.07, 0.07]$. (b) Proposed finite-temperature phase diagram of $\nu \approx 5/2$ quantum Hall states. The thermal metal extends to finite temperatures due to residual interactions between neutral quasiparticles. At higher temperatures, but still below the charge gap, the mechanism discussed here sets in. Near ν^* it results in an large region where κ_{xy} approaches the particle-hole symmetric value 5/2. Hatched regions denote quantization of κ_{xy} that is better than a threshold value, say 1%. The approximate plateaus are separated by relatively sharp crossovers as shown in Fig. 3.

For a clean sample at high temperature, the dephasing length is presumably the shortest scale, and the system's conductance takes the antilocalizing class-D form, where $\kappa_{xx} \propto \log L_\phi/\ell_0$. As the temperature is lowered, we will have $L_\phi > L_E$ and patches of size L_ϕ become large enough for each to manifest a tendency to localization as a system of class A. Thus, in this regime, the conductance decreases with decreasing temperature, with its maximum $\log(D/T\ell_0^2)$ being attained when $L_\phi \approx \sqrt{D/T}$. If phase breaking is sufficiently weak, there will be an intermediate range of temperatures in which $L_\phi > \xi$ and we expect a conductance much smaller than unity. The charge neutrality of the Majorana particles suggests that such a regime may indeed exist. In any case, in the zero-temperature limit the energy dependence of ξ [see Eq. (2)] makes it larger than L_ϕ and the system becomes metallic.

Conclusion.—We have shown that in systems whose effective low-energy theory falls into symmetry class D, increasing temperature can *enhance* quantization of the thermal Hall response. Moreover, new plateaus of quantized κ_{xy} that are absent in the low-temperature limit may emerge and exhibit near-perfect quantization. These findings have direct implications for the interpretation of the measured half-integer values of κ_{xy} in Refs. [12,13].

In the context of the $\nu = 5/2$ plateau, it is not settled whether the observed thermal Hall conductance represents a bulk property or is due to incomplete equilibration between edge states [46–52]. In the former case, the PH-Pfaffian with topologically quantized $\kappa_{xy} = 5/2$, a disorder-induced topological phase with the same quantized value, or a thermal metal where κ_{xy} is not strictly quantized are all possible [15–17]. If particle-hole symmetry were present, it would constrain the Hall response of the thermal metal to be the same as that of PH-Pfaffian. In reality, this symmetry is broken due to relatively strong mixing between Landau levels—the Coulomb energy is comparable to the Landau level splitting in the relevant experiments. Our work shows how an approximately quantized thermal Hall response can emerge with increasing temperature out of a zero-temperature thermal metal whose response is nonquantized. We thus propose that the zero-temperature phase diagram of the quantum Hall state near $\nu = 5/2$ introduced in Refs. [15–17] extends to nonzero temperatures as shown in Fig. 4(b).

More generally, our work emphasizes the importance of systematically measuring the temperature dependence of the approximately quantized κ_{xy}. (In the case of α-$RuCl_3$ the thermal Hall measurements were performed at moderate temperatures of around 4 K.) Theoretically, a careful analysis of dephasing could help determine whether an underlying thermal metal is possible or if the measured κ_{xy} reflects a topological phase.

It is a pleasure to thank Olexei Motrunich, Anton Akhmerov, and Moty Heiblum for illuminating discussions on this topic, and Ulrike Nitzsche for technical assistance. This work was partially supported by the Deutsche Forschungsgemeinschaft (DFG, German Research Foundation) under Germany's Excellence Strategy through the Würzburg-Dresden Cluster of Excellence on Complexity and Topology in Quantum Matter (EXC 2147, Project No. 390858490), through the Collaborative Research Center (CRC) Transregio 183, and through Grants No. EI 519/7-1 and No. MI 658/10-1, by the ERC under the European Unions Horizon 2020 research and innovation programme (Grant Agreement LEGOTOP No. 788715), the BSF and NSF (2018643), the ISF (1866/17), the ISF Quantum Science and Technology (2074/19), and by the German-Israeli Foundation (Grant No. I-1505-303.10/2019).

[1] C. L. Kane and M. P. A. Fisher, Quantized thermal transport in the fractional quantum Hall effect, Phys. Rev. B **55**, 15832 (1997).
[2] D. Arovas, J. R. Schrieffer, and F. Wilczek, Fractional Statistics and the Quantum Hall Effect, Phys. Rev. Lett. **53**, 722 (1984).
[3] G. Moore and N. Read, Nonabelions in the fractional quantum Hall effect, Nucl. Phys. **B360**, 362 (1991).
[4] N. Read and E. Rezayi, Beyond paired quantum Hall states: Parafermions and incompressible states in the first excited Landau level, Phys. Rev. B **59**, 8084 (1999).
[5] N. Read and D. Green, Paired states of fermions in two dimensions with breaking of parity and time-reversal symmetries and the fractional quantum Hall effect, Phys. Rev. B **61**, 10267 (2000).
[6] A. Cappelli, M. Huerta, and G. R. Zemba, Thermal transport in chiral conformal theories and hierarchical quantum Hall states, Nucl. Phys. **B636**, 568 (2002).
[7] B. A. Bernevig and F. D. M. Haldane, Properties of Non-Abelian Fractional Quantum Hall States at Filling $\nu = k/r$, Phys. Rev. Lett. **101**, 246806 (2008).
[8] A. Gromov, G. Y. Cho, Y. You, A. G. Abanov, and E. Fradkin, Framing Anomaly in the Effective Theory of the Fractional Quantum Hall Effect, Phys. Rev. Lett. **114**, 016805 (2015).
[9] K. v. Klitzing, G. Dorda, and M. Pepper, New Method for High-Accuracy Determination of the Fine-Structure Constant Based on Quantized Hall Resistance, Phys. Rev. Lett. **45**, 494 (1980).
[10] S. Jezouin, F. D. Parmentier, A. Anthore, U. Gennser, A. Cavanna, Y. Jin, and F. Pierre, Quantum limit of heat flow across a single electronic channel, Science **342**, 601 (2013).
[11] M. Banerjee, M. Heiblum, A. Rosenblatt, Y. Oreg, D. E. Feldman, A. Stern, and V. Umansky, Observed quantization of anyonic heat flow, Nature (London) **545**, 75 (2017).
[12] M. Banerjee, M. Heiblum, V. Umansky, D. E. Feldman, Y. Oreg, and A. Stern, Observation of half-integer thermal Hall conductance, Nature (London) **559**, 205 (2018).
[13] Y. Kasahara, T. Ohnishi, Y. Mizukami, O. Tanaka, S. Ma, K. Sugii, N. Kurita, H. Tanaka, J. Nasu, Y. Motome, T. Shibauchi, and Y. Matsuda, Majorana quantization and half-integer thermal quantum Hall effect in a Kitaev spin liquid, Nature (London) **559**, 227 (2018).
[14] S. K. Srivastav, M. R. Sahu, K. Watanabe, T. Taniguchi, S. Banerjee, and A. Das, Universal quantized thermal conductance in graphene, Sci. Adv. **5**, eaaw5798 (2019).
[15] D. F. Mross, Y. Oreg, A. Stern, G. Margalit, and M. Heiblum, Theory of Disorder-Induced Half-Integer Thermal Hall Conductance, Phys. Rev. Lett. **121**, 026801 (2018).
[16] C. Wang, A. Vishwanath, and B. I. Halperin, Topological order from disorder and the quantized Hall thermal metal: Possible applications to the $\nu = 5/2$ state, Phys. Rev. B **98**, 045112 (2018).
[17] B. Lian and J. Wang, Theory of the disordered $\nu = \frac{5}{2}$ quantum thermal Hall state: Emergent symmetry and phase diagram, Phys. Rev. B **97**, 165124 (2018).
[18] A. Kitaev, Anyons in an exactly solved model and beyond, Ann. Phys. (Amsterdam) **321**, 2 (2006).
[19] A. Altland and M. R. Zirnbauer, Nonstandard symmetry classes in mesoscopic normal-superconducting hybrid structures, Phys. Rev. B **55**, 1142 (1997).
[20] S. Cho and M. P. A. Fisher, Criticality in the two-dimensional random-bond Ising model, Phys. Rev. B **55**, 1025 (1997).
[21] T. Senthil, M. P. A. Fisher, L. Balents, and C. Nayak, Quasiparticle Transport and Localization in High-T_c Superconductors, Phys. Rev. Lett. **81**, 4704 (1998).
[22] T. Senthil and M. P. A. Fisher, Quasiparticle localization in superconductors with spin-orbit scattering, Phys. Rev. B **61**, 9690 (2000).
[23] M. Bocquet, D. Serban, and M. R. Zirnbauer, Disordered 2d quasiparticles in class D: Dirac fermions with random mass, and dirty superconductors, Nucl. Phys. **B578**, 628 (2000).
[24] J. T. Chalker, N. Read, V. Kagalovsky, B. Horovitz, Y. Avishai, and A. W. W. Ludwig, Thermal metal in network

models of a disordered two-dimensional superconductor, Phys. Rev. B **65**, 012506 (2001).
[25] A. Mildenberger, F. Evers, A. D. Mirlin, and J. T. Chalker, Density of quasiparticle states for a two-dimensional disordered system: Metallic, insulating, and critical behavior in the class-D thermal quantum Hall effect, Phys. Rev. B **75**, 245321 (2007).
[26] F. Evers and A. D. Mirlin, Anderson transitions, Rev. Mod. Phys. **80**, 1355 (2008).
[27] V. Kagalovsky and D. Nemirovsky, Critical fixed points in class D superconductors, Phys. Rev. B **81**, 033406 (2010).
[28] C. R. Laumann, A. W. W. Ludwig, D. A. Huse, and S. Trebst, Disorder-induced Majorana metal in interacting non-Abelian anyon systems, Phys. Rev. B **85**, 161301(R) (2012).
[29] See Supplemental Material at http://link.aps.org/supplemental/10.1103/PhysRevLett.125.236802 for some background on the thermal metal phase of class D systems, the transport geometry used to determine the thermal conductance, numerically obtained conductance scaling plots, as well as the estimated energy dependence of the localization length, which includes Ref. [30].
[30] C. W. Groth, M. Wimmer, A. R. Akhmerov, and X. Waintal, Kwant: A software package for quantum transport, New J. Phys. **16**, 063065 (2014).
[31] B. Kramer and A. MacKinnon, Localization: Theory and experiment, Rep. Prog. Phys. **56**, 1469 (1993).
[32] S. Hikami, A. I. Larkin, and Y. Nagaoka, Spin-orbit interaction and magnetoresistance in the two dimensional random system, Prog. Theor. Phys. **63**, 707 (1980).
[33] Y. Asada, K. Slevin, and T. Ohtsuki, Anderson Transition in Two-Dimensional Systems with Spin-Orbit Coupling, Phys. Rev. Lett. **89**, 256601 (2002).
[34] Y. Asada, K. Slevin, and T. Ohtsuki, Numerical estimation of the β function in two-dimensional systems with spin-orbit coupling, Phys. Rev. B **70**, 035115 (2004).
[35] H. Obuse, A. Furusaki, S. Ryu, and C. Mudry, Two-dimensional spin-filtered chiral network model for the $\mathbb{Z}_2$ quantum spin-Hall effect, Phys. Rev. B **76**, 075301 (2007).
[36] Z. Wang, M. P. A. Fisher, S. M. Girvin, and J. T. Chalker, Short-range interactions and scaling near integer quantum Hall transitions, Phys. Rev. B **61**, 8326 (2000).
[37] D. T. Son, Is the Composite Fermion a Dirac Particle?, Phys. Rev. X **5**, 031027 (2015).
[38] S.-S. Lee, S. Ryu, C. Nayak, and M. P. A. Fisher, Particle-Hole Symmetry and the $\nu = 5/2$ Quantum Hall State, Phys. Rev. Lett. **99**, 236807 (2007).
[39] M. Levin, B. I. Halperin, and B. Rosenow, Particle-Hole Symmetry and the Pfaffian State, Phys. Rev. Lett. **99**, 236806 (2007).
[40] Y. f. Yang, G.-M. Zhang, and F.-C. Zhang, Universal Behavior of the Thermal Hall Conductivity, Phys. Rev. Lett. **124**, 186602 (2020).
[41] Neither symmetry is related to the intrinsic PH symmetry of BdG Hamiltonians, which does not impose any such constraint.
[42] I. V. Lerner and Y. Imry, Magnetic-field dependence of the localization length in Anderson insulators, Europhys. Lett. **29**, 49 (1995).
[43] W. Long, H. Zhang, and Q.-F. Sun, Quantum thermal Hall effect in graphene, Phys. Rev. B **84**, 075416 (2011).
[44] J. M. Ziman, *Electrons And Phonons: The Theory of Transport Phenomena in Solids*, Oxford Classic Texts in the Physical Sciences (Oxford University Press, New York, 2001).
[45] Y. Imry, *Introduction to Mesoscopic Physics* (Oxford University Press, New York, 1997).
[46] S. H. Simon, Interpretation of thermal conductance of the $\nu = \mathbf{5/2}$ edge, Phys. Rev. B **97**, 121406(R) (2018).
[47] D. E. Feldman, Comment on "Interpretation of thermal conductance of the $\nu = 5/2$ edge", Phys. Rev. B **98**, 167401 (2018).
[48] S. H. Simon, Reply to "Comment on 'Interpretation of thermal conductance of the $\nu = 5/2$ edge'", Phys. Rev. B **98**, 167402 (2018).
[49] K. K. W. Ma and D. E. Feldman, Partial equilibration of integer and fractional edge channels in the thermal quantum Hall effect, Phys. Rev. B **99**, 085309 (2019).
[50] S. H. Simon and B. Rosenow, Partial Equilibration of the Anti-Pfaffian Edge due to Majorana Disorder, Phys. Rev. Lett. **124**, 126801 (2020).
[51] H. Asasi and M. Mulligan, Partial equilibration of anti-Pfaffian edge modes at $\nu = 5/2$, Phys. Rev. B **102**, 205104 (2020).
[52] J. Park, C. Spånslätt, Y. Gefen, and A. D. Mirlin, Noise on the Non-Abelian $\nu = 5/2$ Fractional Quantum Hall Edge, Phys. Rev. Lett. **125**, 157702 (2020).